Journal of Photochemistry and Photobiology A: Chemistry 353 (2018) 358–367

Contents lists available at ScienceDirect

Journal of Photochemistry and Photobiology A: Chemistry

journal homepage: www.elsevier.com/locate/jphotochem

High-performance ultraviolet-visible driven ZnO morphologies photocatalyst obtained by microwave-assisted hydrothermal method

Gabriela Byzynski[a,*], Andreza Prado Pereira[b], Diogo P. Volanti[b], Caue Ribeiro[c], Elson Longo[d]

[a] IQ, UNESP – São Paulo State University (Unesp), Araraquara, SP, Brazil
[b] IBILCE, UNESP – São Paulo State University (Unesp), S. J. Rio Preto, SP, Brazil
[c] EMBRAPA INSTRUMENTAÇÃO, São Carlos, SP, Brazil
[d] DQ, UFSCar – Universidade Federal de São Carlos, São Carlos, SP, Brazil

ARTICLE INFO

Article history:
Received 12 June 2017
Received in revised form 15 November 2017
Accepted 18 November 2017
Available online 22 November 2017

Keywords:
ZnO
Morphology
Controlled synthesis
Oxygen vacancy
Visible photocatalysis

ABSTRACT

The use of extensive, time-consuming synthesis and the cost of an additional element in synthesis makes difficult the synthesis of photocatalyst active under a broad wavelength range. We propose a synthesis method to obtain ZnO nanoparticles in distinctive morphologies, which lie to several photocatalytic activation conditions. The Zn precursor concentration, solvent, temperature and reaction time altered the ZnO particles morphologies. Although all synthesis parameters modification interferes in ZnO particle morphology, the most pronounced was Zn salt precursor concentration. The synthesis parameter did not interfere in the crystalline wurtzite ZnO phase and the optical characterization, indicating possibilities of ionic defects formations in ZnO lattice. The "3-D flower like" ZnO structure reaches 98% of discoloration under UV illumination and 42% under visible illumination of initial rhodamine-B concentration. The good UV and visible photocatalytic active confirms that with only the modification of synthesis method without any dopant element, ZnO structure is active in large wavelength range.

1. Introduction

Besides the use as semiconductor, Zinc oxide (ZnO) deserves to be highlighted in other fields such as photocatalysis [1], solar cells [2], gas sensors [3], optical sensors [4], etc. The most abundant structure of ZnO is the hexagonal wurtzite, presenting a band gap value of 3.37 eV (368 nm) and excitation of 60 meV [5]. The morphological properties of ZnO are influenced by synthesis method used and the modification of some parameters, such as the concentration of dopants and substituents among others, may affect the photocatalytic behavior of the semiconductor. Thus, the same material obtained by different methods may present appropriate modifications, since the crystalline structure, morphology, and composition of the material may vary according to the preparation method [6,7].

The concentration of precursor reactants, reaction temperature, and reaction time, as well as the possibility of using surfactant during the synthesis, are important factors in influencing the growth of the ZnO crystals. Komarneni et al. [8] observed that the use of microwave radiation in a hydrothermal system increases the crystallization kinetics compared to the conventional hydrothermal system. The interaction of high frequencies of electromagnetic radiation with the permanent dipole of the solvent molecules, which reaches high temperatures in a short period due to the molecular rotation, occurs with the use of microwave radiation. The microwave assisted hydrothermal method has advantages such as short time reaction, convenience and low cost effective, besides the possibility of obtaining particles of different morphologies [8–10].

The synthesis method could alter the oxygen vacancies density on the material, modifying the photocatalyst proprieties as a photocatalytic activity. The interstitial zinc and oxygen vacancies are well known as the mainly ionic defects in ZnO crystalline lattice structure and also could be caused by the addition of impurities elements (dopants). However, the synthesis conditions could introduce some defects, without the use of extras reagents. In the case of ZnO, there are some defects states within the ZnO band gap, as donor defects (Zn_i^x, $Zn_i^{\bullet}$, $Zn_i^{\bullet\bullet}$, V_o^x, $V_o^{\bullet}$, $V_o^{\bullet\bullet}$) or acceptor defects (V_{Zn}',V_{Zn}''), presenting ionization energies between 0.05–2.8 eV [11].

* Corresponding author.
E-mail address: gabi.byzynski@gmail.com (G. Byzynski).

https://doi.org/10.1016/j.jphotochem.2017.11.032
1010-6030/

The mechanisms of photocatalytic activity of the ZnO particles have been proposed by others [12–15]. On the basis of our previous study [16], according to Kroger-Vink notations and cluster model [17,18], ZnO structure is ideally constructed by four folder tetrahedron, denoted as $[ZnO_4]^x$. Considering the ZnO an intrinsically *n*-type semiconductor, the presence of intrinsic defects could occur as zinc interstitials, zinc vacancies, and oxygen vacancies. It is generally accepted that, the photoelectron produced by nanocrystals irradiation can be easily trapped by electronic acceptors, whereas the photoinduced holes can be trapped by electronic donors. The type and concentration of oxygen defects on the surface and/or surface layer influences in the photocatalytic activity [19–21]. The oxygen vacancies created during the synthesis in the ZnO structure, could be in three different situations: neutral (V_o^x), mono-ionized ($V_o^\bullet$), and de-ionized ($V_o^{\bullet\bullet}$). In photocatalytic process (Fig. 1), an incident photon with energy equal or higher than band gap energy of the photocatalyst, is absorbed by $[ZnO_4]^x$ structure, generating a negative charge ($[ZnO_4]$) or electrons in CB and a positive charge ($[ZnO_3.V_o^\bullet]$) or holes in VB [7,11,16,22].

$$[ZnO_4]^x + [ZnO_3.V_o^x] \rightarrow [ZnO_4]' + [ZnO_3.V_o^\bullet] \quad (1)$$

The both charge should be moved until the photocatalyst surface to promote the sequent redox reaction if there are molecules adsorbed which will receive or donate negative charge. If those molecules are not present, the recombination event takes place in nanoseconds, decreasing the photocatalytic performance of the material. Molecular oxygen adsorbed in photocatalyst surface could be associated with the negative charge, $[ZnO_4]'$, producing $O_2H^\bullet$ radicals.

$$[ZnO_4]' + O_2 \rightarrow [ZnO_3.V_o^x] \ldots O_{2(ads)}' \quad (2)$$

$$[ZnO_3.V_o^x] \ldots O_{2(ads)}' + H^\bullet \rightarrow [ZnO_3.V_o^x] \ldots O_2H^\bullet_{(ads)} \quad (3)$$

In the same way, adsorbed water molecules react with mono-ionized oxygen vacancies, $[ZnO_3.V_o^\bullet]$, producing $OH^\bullet$ radicals, which with $O_2H^\bullet$ radical, play an important role in the organic substance degradation.

$$[ZnO_3.V_o^\bullet] \ldots OH_{2(ads)} \rightarrow [ZnO_3.V_o^x] \ldots OH^\bullet_{(ads)} + H^\bullet \quad (4)$$

Under visible illumination, it is well known and accept that the dye sensitizing mechanism could occur [23,24], enable that an exciting RhB molecule (RhB*) react with ZnO structure ($[ZnO_4]^x$), generating negative charge ($[ZnO_4]'$) or electrons in CB. After $[ZnO_4]'$ creation, the sequence reactions as Eqs. (2) and (3) are promoted.

$$[ZnO_4]^x + RhB^\bullet \rightarrow [ZnO_4]' \ldots RhB^\bullet_{(ads)} \rightarrow [ZnO_4]' + RhB^\bullet \quad (5)$$

This work has the objective of obtaining different ZnO photocatalytic materials through the variation of synthesis parameters such as reagent concentration, solvent change, temperature and reaction time of synthesis, using the microwave-assisted hydrothermal method. The characterization of the main crystalline phase, optical behavior and morphology were performed. The photocatalytic activity of the different samples was also evaluated, being photocatalysis efficiencies related to the modifications caused by the variation of synthesis parameters.

2. Materials and Methods

2.1. Synthesis of ZnO materials

The samples were synthesized by microwave-assisted hydrothermal method (MAH), with the change of some synthesis parameters as initial concentration of the zinc precursor (zinc acetate – $C_4H_6O_4Zn$ – Sigma-Aldrich, >98%), the influence of the solvent, temperature and time of synthesis, as presented in Table 1. Basically, with constant stirring of 30 mL of zinc acetate solution

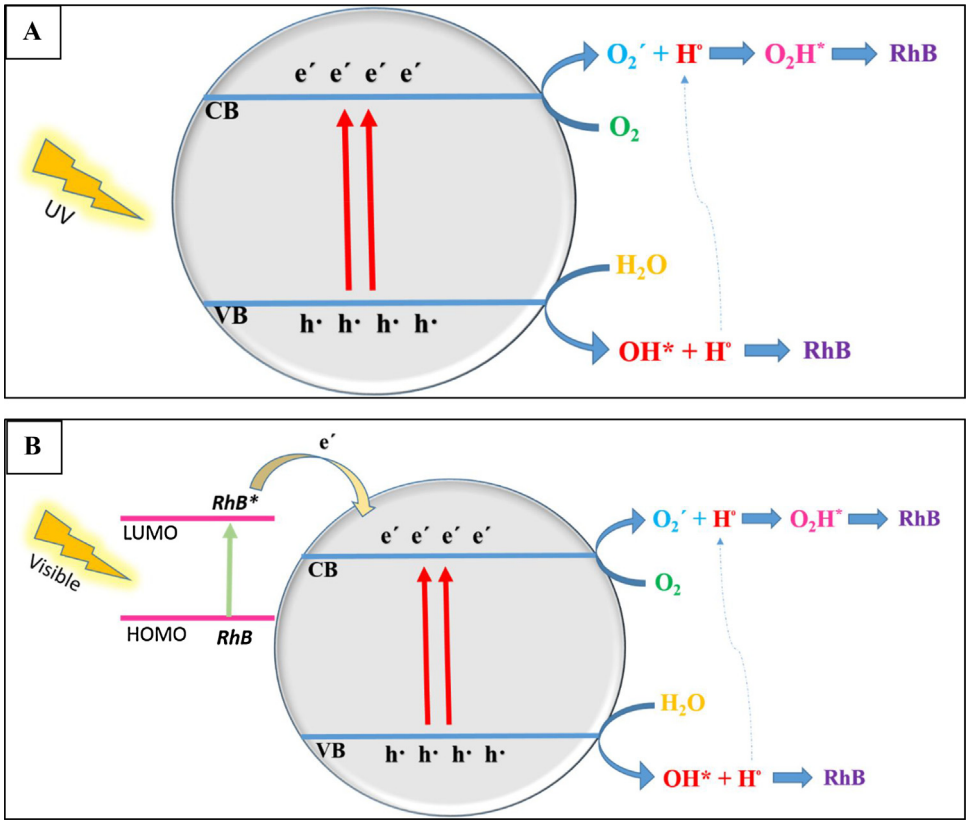

Fig. 1. Scheme of the photocatalytic mechanism proposed by ZnO samples under UV illumination (A) and visible illumination (B).

Table 1
Synthesis parameters of ZnO materials by the microwave-assisted hydrothermal method.

Sample	*Precursor (mol L^{-1})*	*Solvent*	*Temperature (°C)*	*Reaction Time (minutes)*
Plates (PL)	0.027	water	100	60
Rounded Plates (RP)	0.027	water/ethyl alcohol (50/50 v/v)	100	60
Brush-Like (BL)	0.027	water	140	45
Flower-Like (FL)	0.016	water	100	60

during 10 min, 10 mL of NaOH solution (2 mol L^{-1}) is slowly dropped to ensure that the reaction between Zn^{2+} and OH^- reaches equilibrium, according to Eq. (6):

$$Zn^{2+} + 4OH^- \leftrightarrow Zn(OH)_4^{2-} \leftrightarrow ZnO + H_2O + 2OH^- \quad (6)$$

The pH of the solution is about 10 and pH variation was not performed. The resulting solution was used in polytetrafluoroethylene (PTFE) reactor and kept under microwave irradiation (800W) [25]. The obtained solution was centrifuged and washed (5 x) with deionized water. The resulted powder was dried at 80 °C overnight. The samples were named based on the morphology as described in Table 1, as plates (PL), rounded plates (RP), brush-like (BL), and flower-like (FL).

2.2. Characterization techniques

Powder morphology and size was characterized by field emission scanning electron microscopy (FE-SEM) with JEOL Microscope – —Model JSM 6701F. The X-ray powder diffraction (XRD) patterns obtained with Higaku MiniFlex 300 diffractometer (Cu Kα radiation (λ = 1.5418 Å), scanning from 2θ of 20° to 80°, at 2° min^{-1}) were used to obtain the samples phase composition and crystalline structure. Search Match software was used to indexed the crystallographic phase. N_2 physisorption (Micromeritics Germini VII) was used to obtain the surface areas (SA) of the synthesized samples, using the Brunauer- Emmett-Teller (BET) method. The ultraviolet–visible–near infrared (UV– vis–NIR Cary 5G spectrophotometer) in diffuse reflectance mode was utilized by optical properties evaluation. Photoluminescence emission spectra were obtained in ThermoScientific Fluorimeter with an excitation wavelength of 350 nm, excitation slit of 10 nm, emission slit of 20 nm and scan speed of 2400.

Electrochemical measurements were carried out in a conventional three-electrode system, connected to a computer-controlled potentiostat (MQPG-01- Microchimica), with a thin film electrode as working electrode, Saturated Calomel Electrode (SCE) as the reference electrode, and a Pt wire as the counter electrode. The thin film electrode was produced by dip coating an ITO (indium-tin oxide) substrate with the solution of synthesized materials dispersed in ethylene glycol (2 mg/mL). The area of thin film electrodes were 270.75 mm^2. Cyclic voltammograms were measured in a 0.005 mol L^{-1} aqueous solution of potassium ferricyanide ($K_3Fe(CN)_6$)(Merck) and Na_2SO_4 (0.1 mol L^{-1})(Merck), with a scan rate of 50 mV s^{-1}.

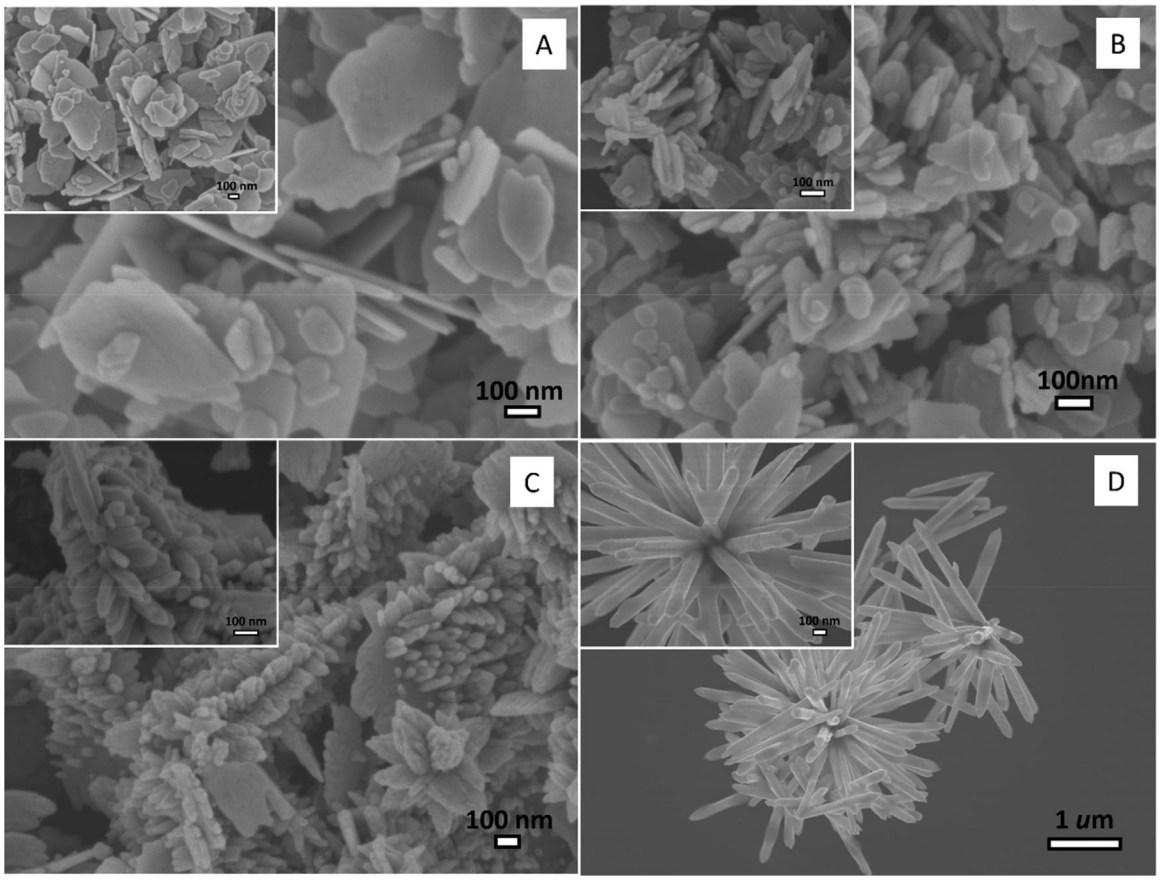

Fig. 2. FEG-SEM images of PL (A), RP (B), BL (C), FL (D)ZnO obtained samples.

Photocatalytic studies were done for the discoloration of rhodamine-B (RhB) (2.5 mg L^{-1}) dye solution. 2 mg of each powder sample was dissolved in 20 mL of RhB solution, in a separate beaker, under magnetic stirring. The solutions were then illuminated with six UVC lamps (TUV Philips, 15W, with maximum intensity at 254 nm), during two hours, with magnetic stirring at a constant temperature of 25 °C, and aliquots were taken at intervals of 30 min. A UV–vis spectrophotometer (Shimadzu-UV- 1601 PC spectrophotometer) was used to monitor modifications in optical absorption of the resultant solutions throughout the experiment. A similar procedure was repeated using a visible light source (six Philips lamps, 15W, and maximum intensity at 440 nm). Control, without catalysts, was also performed (photolysis). RhB photodiscoloration was conducted on the average of triplicate. Adsorption experiments were carried out similarly to photocatalytic studies without illumination.

3. Results and discussion

3.1. Morphology evaluation

The modifications in the synthesis conditions as solvent, temperature, and reaction time, can affect the morphology of the samples, as presented by the FEG-SEM images (Fig. 2). First of all, the solvent synthesis was not significant in morphological modification since Plates (PL), and Rounded Plates (RP) samples depict similar morphologies, with comparable particle agglomeration in plates forms with different sizes (Fig. 2A, and B). PL sample shows the same synthesis condition as RP sample, except by the solvent used (Table 1). The aqueous solvent is well known as indicating a higher dielectric constant (80.4) compared with ethyl alcohol solvent (25) [26,27]. The plates thickness is slightly altered by changing the dielectric constant through solvent modification. With only aqueous solution as the solvent reaction (PL sample), the thickness can vary from 22 to 37 nm. With aqueous solution and ethyl alcohol as a solvent reaction (RP sample), the thickness of the plates decreases (13–29 nm), due to the decrease in dielectric constant of the resulted solvent. As lower the dielectric constant of the medium, the attraction forces between cations and anions diminished, resulting in secondary particles sizes. On the other hand, it also influences the steric hindrance due to the ethyl group, which decreases the number of effective shocks in the formation of the crystal. On the other hand, the concentration of initial zinc precursor is responsible for a substantial morphological modification (Fig. 2A, and D). PL sample presents the same synthesis condition as a Flower-like sample (FL), except by the zinc precursor concentration (Table 1).

The FL sample presents morphology characterized by nanorods of large size and thickness, with the convalescent site, that is, the growth of these nanorods occurs from a common point, forming a 3D flower-like structure. The presence of some non-convalescent nanorods, as disperse nanorods are observed. This structure is well known in the literature for semiconductor materials obtained by the microwave-assisted hydrothermal method [16,28–31].

As previously discussed, the modification in medium dielectric constant by solvent change does not play a major role in morphological alteration as comparing FL and RP samples. A test sample (TS), with the same zinc precursor, temperature and time reaction as FL sample, was obtained only to confirm the major influence of zinc precursor solution instead of a solvent change in the morphological structure. The only difference between TS and FL samples is the solvent, which in TS sample is ethyl alcohol. With the use of ethyl alcohol as solvent (Fig. 1–Supporting information), the morphology of the particles was not changed compared to FL sample. However, the size and thickness of ZnO nanorods reduced and the reaction yield is insufficient (<10%). In this way, the amount of zinc precursor in solution interferes in growth ZnO particle mechanism more than the solvent reaction. TS sample was only used in morphological comparison with FL sample, and the characterization properties for TS sample will not take into account.

The temperature and reaction time also influenced in ZnO morphologies. The Brush-like (BL) sample was obtained in superior temperature and diminished reaction time than FL. Comparing FL with BL sample (Fig. 2A and C), even the zinc precursor concentration was high in the reaction solution, the self-assembly of nanowires formation is evident, convalescent along one same axis, and known as "3-D Brush-like". Due to the high zinc precursor concentration in the solution, there are still some formations of ZnO particle agglomerates as plate structure, where there is located normal growth of nanorods, not exhibiting morphological homogeneity.

It is evident that the synthesis process by MAH method with more elevated temperature (140 °C) accelerates the ZnO microwires particles formation, even in a short reaction time (45 min). In this case, it was not necessary diluted zinc precursor solution in synthesis to produce wires-like structures. Wang [32] presented a similar result observed for BL sample, where the rapid growth of axial ZnO wires or rods along the face [0001] and, in a second step, the formation of rods of ZnO in the directions ± [1010], ± [0110] and ± [1100]. It is thus possible to confirm that the concentration of the precursor solution, as well as the time and temperature of synthesis, can affect the morphological structure due to the crystal growth mechanism of the ZnO particles.

3.2. X-ray diffraction

Fig. 3 shows X-ray diffraction patterns of the ZnO samples. The diffractograms are similar for samples as the crystallographic phase of hexagonal structure ZnO wurtzite (JCPDF 36-1451). There are no crystallographic peaks of contaminations identified diffractograms. The alteration of the synthesis conditions, as temperature and reaction time, and not even the alteration of the synthesis solvent, changes the main crystalline phase of each sample. This result indicates the possibility of obtaining the crystalline ZnO phase in a low period and soft temperatures.

3.3. Optical behavior

With the morphological alteration, some properties can be modified as optical behavior and photocatalytic efficiency of the

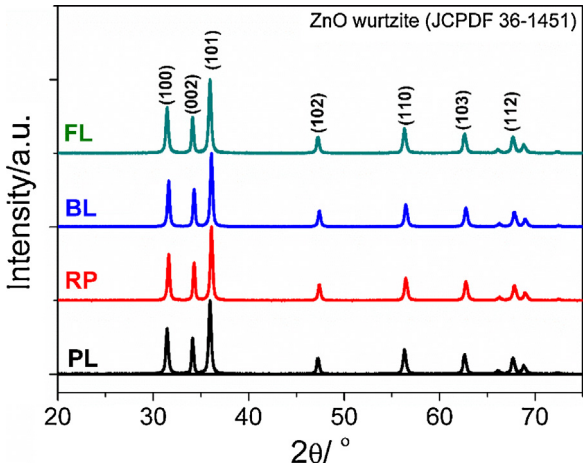

Fig. 3. X-ray diffractograms of ZnO samples obtained by microwave-assisted hydrothermal methods.

material. Thus, the properties of the samples were evaluated. The optical behavior of the ZnO samples was assessed by UV–vis diffuse reflectance spectroscopy (DRS). Fig. 4 shows the DRS spectra for PL, RP, BL, and FL samples, where it is possible to observe an intense band around 380 nm, being attributed to the intrinsic band gap absorbance of ZnO crystalline particles. The characteristic absorption intensity of ZnO nanoparticles in UV light region, in Fig. 4, suffers influences of the different scattering events of ZnO samples, related to diverse morphology, sizes, shapes and crystalline quality of the material, which is induced by synthesis conditions as precursor concentration, solvent, temperature, and reaction time.

The DRS results were used to calculate the band gap values of the semiconductor for each sample, using the Kubelka-Munk model [33]. The calculated band gap values for the samples show small deviations from the values of the literature [34–36] (Table 2), which indicates an approximate gap of 3.2 eV. Band gap values samples differ from band gap values obtained for samples synthesized by solvothermal method (E_{bg} = 3.31 eV) and for ZnO quantum dots (E_{bg} = 3.41–3.47 eV) [36]. The BL sample, synthesized in a shorter time and higher temperature, shows the largest divergence band gap values from other ZnO samples. The synthesis condition promotes a defects density [37] more elevated in BL sample compared to the others, decreasing, even more, the band gap value. Thus, it is possible to confirm that the synthesis conditions, such as time and temperature, is a major factor in the optical properties of ZnO particles and could obtain different photocatalytic performance.

Fig. 5 shows the photoluminescence emission spectra of samples, indicating a peak about 570 nm. As the excitation wavelength was similar with a band gap energy (350 nm), the peak presented in emission spectra could be ascribed to the band gap-free excitation due to indirect transition. Trapped surface states in the material are correlated with the indirect transition and as higher the photoluminescence emission intensity, the recombination efficiency of photogenerated carrier increases [25]. According to Fig. 5, the intensity of PL emission spectra of RP sample is the highest one, followed by PL, FL, and BL, that represent photogenerated electron/hole recombination is higher for RP and PL sample. For FL and BL, the photogenerated electron/hole recombination decreases. The photo-charge carrier recombination promotes a decline of the photocatalytic efficiency, as inhibiting the radical production resulted by the photo charge carrier trap. It is interesting to notice that the photo-charge recombination of Plates and Rounded Plates morphologies show more elevated than

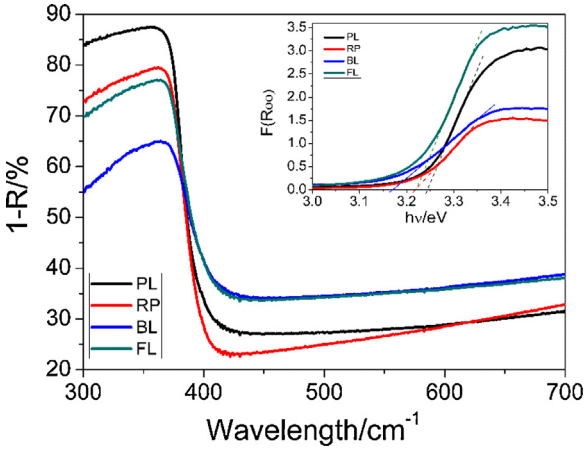

Fig. 4. Diffusive reflectance spectra of ZnO samples. Insert: Kubelka Munk function vs. band gap energy for ZnO morphologies (PL, RP, BL, FL samples).

Table 2
Band gap values and Superficial surface area of ZnO samples.

Samples	*Band gap values (eV)*	*Superficial Surface Area ($m^2 g^{-1}$)*
Plates (PL)	3.24	10.70 ± 0.40
Rounded Plates (RP)	3.21	9.18 ± 0.49
Brush-Like (BL)	3.17	9.49 ± 0.54
Flower-Like (FL)	3.22	8.46 ± 0.68

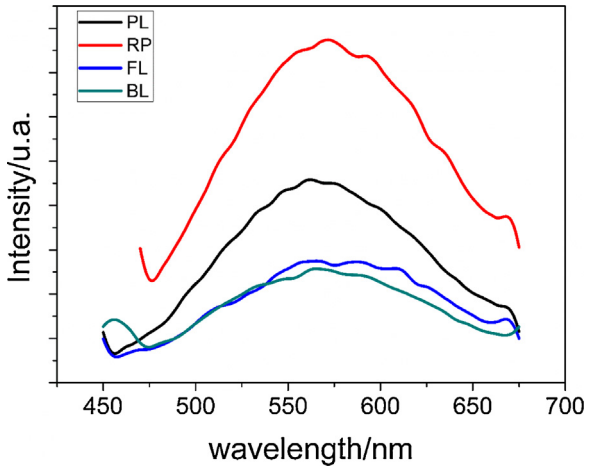

Fig. 5. Photo-fluorescence emission spectra with excitation at 350 nm of the samples.

for Brush-like and 3-D flower-Like morphologies, indicating a possible influence of morphology in the recombination process.

3.4. Photoelectrochemical behavior

Cyclic voltammogram (CV) of thin-film electrodes constructed with each sample was used to obtain the standard heterogeneous rate constant, k_0, which corresponds to the rate of electron transfer. Standard heterogeneous rate constant was obtained by Nicholson method [38]. Fig. 6 presents the CVs of each sample in the dark and under UV illumination (photocurrent), indicating a similar electrochemical behavior between samples. Table 3 presents the peak-to-peak potential separation (ΔV) and the peak density of each material. Compared the CVs of all samples, one can notice that the synthesis condition could influence the capacitive behavior of the ZnO materials. The PL sample presents the highest oxidative, and reductive peak density and BL sample depicts the lowest one in dark conditions. The illumination provokes an increase in photocurrent in oxidative density and PL and FL reduction density. Also, the illumination promotes an enlargement in ΔV for PL and RP samples and a diminution for BL and FL samples. For k_0 calculation, the diffusion coefficients was adopted as $D_O = D_R = 7.26 \times 10^{-6}\,cm^2\,s^{-1}$ and k_0 values are showed in Table 3. The k_0 values were slightly close for samples PL, RP and BL. FL sample shows an elevated value of 2.29, indicating an increase in electron transfer in the electrode with appropriate potential gradient, which could be promoted by the organized material morphology. Then, the faster electron transfer with lower photogenerated carrier recombination indicates advantages in photocatalytic activity.

The potential that no charge transference occurs is known as the flat band potential (V_{fb}) and is defined by Buttler equation for

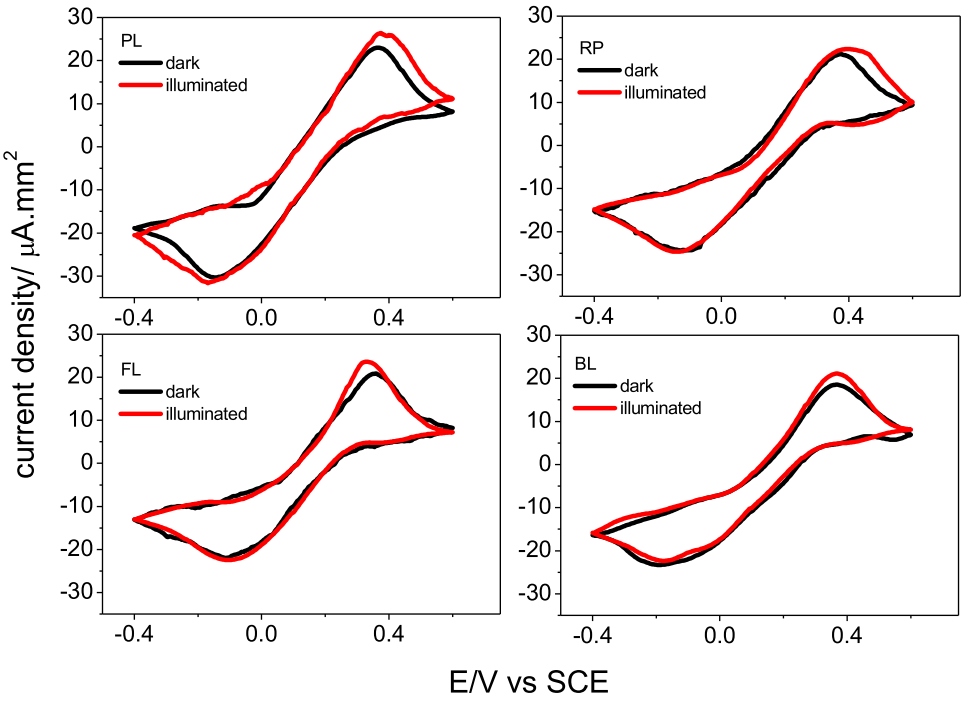

Fig. 6. Cyclic voltammograms of ZnO thin-film electrodes in the dark and with UVC illumination. Scan rate = 50 mV s^{-1}; electrolyte solution: $(K_3Fe(CN)_6)$, 0.005 mol L^{-1} at ambient temperature.

Table 3
Peak-to-peak separation (ΔE) values, the current density of oxidation (i_{oxi}) and reduction (i_{red}) obtained from Fig. 5 and the standard heterogeneous rate constant (k_0).

Samples	*ΔV (V vs SCE)*	i_{oxi} ($\mu A\,mm^{-2}$)	i_{red} ($\mu A\,mm^{-2}$)	$k_0\ 10^2$ ($cm\ s^{-1}$)
Plates (PL) - dark	0.508	21.61	−19.11	
Plates – UV	0.548	23.32	−19.39	1.71
Rounded Plates (RP) - dark	0.478	17.53	−16.88	
Rounded Plates – *UV*	0.537	18.66	−16.62	1.75
Brush - Like (BL) - dark	0.541	17.07	−13.11	
Brush-like – UV	0.539	18.74	−12.89	1.75
Flower - Like (FL) - dark	0.455	18.43	−15.99	
Flower like – UV	0.427	22.94	−16.86	2.29

each semiconductor.

$$j^2 = \left(\frac{2q\varepsilon\varepsilon_0 I_0^2 \alpha^2}{N_d}\right)(V - V_{fb}) \quad (7)$$

where j is the photocurrent density, ε is the permittivity of the surroundings, ε_0 is the vacuum permittivity, I_0 is the current density difference, α is the optical absorption coefficient, N_d is the number of charges donors, q is the transferred charge per ion, V is

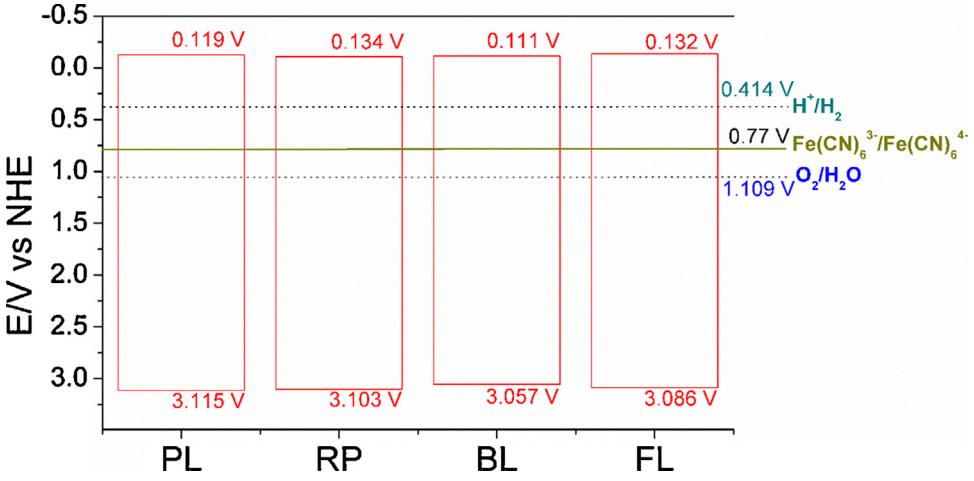

Fig. 7. Schematic energy band diagrams obtained through CVs and band gap values results for ZnO samples.

the potential [38]. The flat band potential is obtained with the x-axis onset of the square photocurrent in Fig. 6. For an *n*-type semiconductor, the flat band potential is similar with conduction band edge, and it is possible to construct the band diagram of the material (Fig. 6), adding the band gap values to CB edge. The CB edge is similar to all the samples. However, the methods conditions could influence in valence band edge as indicated in Fig. 7. Not only doping or heterostructure construction could vary the band diagram of such material [39,40], but also the synthesis condition as precursor concentration, time and temperature of the synthesis reaction.

3.5. Photocatalytic performance

The photocatalytic activity of the samples was evaluated by the photo-discoloration of RhB solution under UV and visible illumination (Fig. 8A and B). Table 4 presents the values of the kinetic constants for each material, adopting the reaction of pseudo-first order [7], normalized by proportional semiconductor area used in each experiment. As for each photocatalytic experiment, a defined mass of semiconductor was used, the proportional semiconductor could be obtained multiplying the Superficial Surface Area (SSA – Table 2) and the semiconductor mass. Considering the first step of photocatalysis process is an adsorption of RhB in active sites of semiconductor, isothermal adsorption experiment in the absence of illumination was carried out in the dark condition (Figure SI-2). The removal percentage of RhB by the adsorption in two hours was calculated using the (C_0 – Ct)/C_0 equation, where C_t and C_0 are the equilibrium and initial concentration of RhB in the solution (mg L^{-1}), respectively. The PL sample revealed a minimum RhB-adsorption percentage of about 2%, while the RP revealed a maximum RhB-adsorption proportion of about 6%. Based on the experimental results, the degradation is mainly dominated by the photochemical reaction, not adsorption.

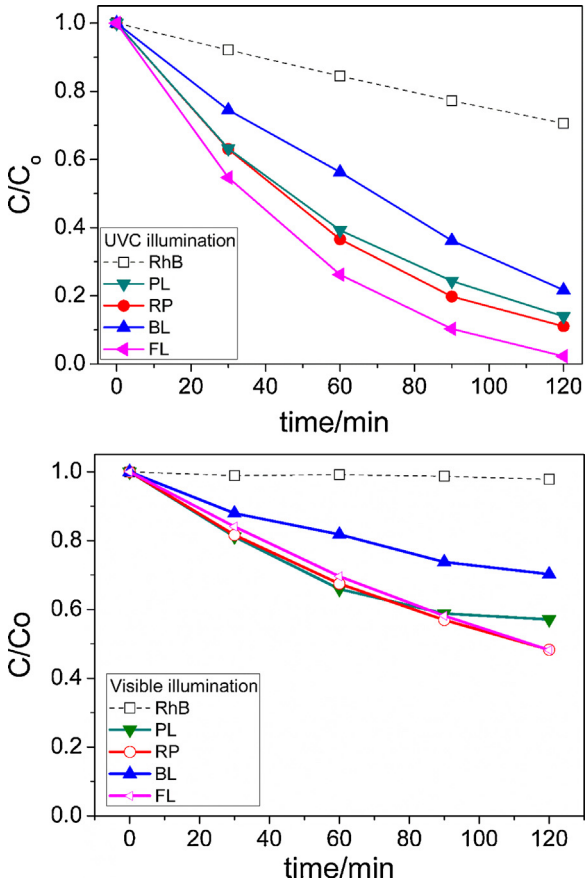

Fig. 8. Kinetic of RhB photo-discoloration under UVC (A) and visible illumination with ZnO samples synthesized (B).

Table 4
Kinetic constants of RhB degradation under UVC and visible illumination for ZnO synthesized samples. The k values obtained was normalized by the SSA and semiconductor weight used in photocatalytic experiment. R^2 values indicate the adjustment of the kinetic order consideration (pseudo-first order reaction).

Samples	*k x 10^{-2} (g min^{-1})* UVC illumination	R^2	*k x 10^{-3} (g min^{-1})* Visible illumination	R^2
Plates (PL)	*109.35 ± 7.94*	0.980	*226.64 ± 35.51*	0.909
Rounded Plates (RP)	*101.31 ± 3.27*	0.996	330.61 ± 9.26	0.997
Brush-Like (BL)	*37.93 ± 1.58*	0.994	129.08 ± 6.32	0.990
Flower- Like (FL)	*184.09 ± 20.19*	0.954	359.26 ± 4.75	0.999

The kinetic profile (Fig. 8) shows the photocatalytic potential of the samples, and it is also possible to confirm that the variations of the synthesis conditions directly influence the photocatalytic properties of the samples, since modification in synthesis condition alters the materials properties as presented later.

The FL sample is more efficient for the application in UVC illumination photocatalysis (Fig. 8A) reached 98% of RhB solution during 120 min. Moreover, the synthesis of ZnO in an aqueous medium at 100° C for 1 h, with a lower concentration of precursor solution, results in particles of ZnO more photoactive under UVC illumination. The photocatalytic process is influenced by morphological variation. Due to the different kinetic factors (a type of precursors, concentration, solvent, and synthesis method), the crystals formed have different morphologies. These different morphologies are formed of distinct surfaces and concentration of various defects. This fact induces the formation of surface clusters, with various electron-hole density, modifying the band gap of the surface. The band gap value expresses the energy quantity required to transfer, with a photon, one electron from valence band (VB) to the conduction band (CB) of the semiconductor and, is another factor that affects the photocatalytic active, mainly in visible light illumination. However, FL sample presents the lowest superficial surface area (Table 2) and the band gap value of 3.22 eV. However, the FL sample presents “3-D flower-like” morphology, with some dispersed nanorods and compared with other samples, FL sample presents a more organized structure morphology, corroborating with effective photo-charge carriers (electrons/hole) separation, indicated by photoluminescence experiment. When an electron is photo-excited in CB to VB, it is created a hole (positive charge) in VB. If there is no receptor molecule for electron or hole under the surface of the semiconductor, the photo-charge recombination occurs. In the case of FL sample, the photo-charge separation is effective, resulting in a decrease of photo-charge recombination, promoting a favorable condition for efficient photocatalysis.

The influence of the addition of ethanol on ZnO synthesis (RP sample) did not affect the photocatalytic efficiency, being similar to an aqueous solution (PL sample) from the kinetic point of view under UVC illumination (Table 4). R^2 values presented in Table 4 indicate the adjustment of the kinetic order consideration, as pseudo-first order reaction. PL sample reached 86% of RhB solution discoloration, and RP sample obtained 89% of RhB discoloration during 120 min. PL and RP samples present similar morphologies structure, like plates with different sizes. The only difference is that PL sample presents plates with more elevated sizes than RP. Though the SSA of PL sample is higher than the RP sample (Table 2),

could be promoted improve in photocatalytic activity, the band gap value of RP sample is lower than the PL sample. The photo-generated carrier recombination is more elevated for RP than for PL, and the electron transfer is similar.

On the other hand, the influence of zinc precursor salt in photocatalytic performance is noticeable (Table 4). The PL sample (89% RhB discoloration), with more concentrated precursor solution, shows lower photocatalytic activity than FL sample (98% RhB discoloration), with diluted precursor solution. Although the samples proprieties were different (PL and FL samples), the morphology plays a major role in the photocatalytic performance of samples. However, the electrical properties as charge recombination and electron transfer also influence in the photocatalytic efficiency, as previously described.

The BL sample, synthesized at a higher temperature and lower reaction time, without alteration of the concentration of precursor solution comparing with PL, presents a lower photocatalytic efficiency (Table 4), obtaining 78% of RhB discoloration during 120 min. The SSA of BL sample (Table 2) is the second largest compared to others and could not favor the photocatalytic performance. The BL sample presents diverse structures in morphology characterization, presenting nano-wires convalescents under a same line and plates, where nanowires growth under them. With morphology disorganization, photocatalytic performance could be negatively influenced with photo-charge carrier recombination. The band gap value of BL is the lowest value, and electron transfer rate and photo-charge carrier recombination are small.

As the surface area influences the photocatalytic activity, due mainly to different morphologies and crystal growth mechanisms for each sample presented, the crystalline faces, as well as the orientation of the ZnO crystal, also influence the photocatalytic activity of the samples [41]. Pung et al. [42] showed the photocatalytic efficiency of different ZnO particles as a plate, rice and stick morphologies. The last morphology showed a higher photocatalytic activity under UVC illumination, followed by the sample with “rice-like” and plates ZnO morphologies. The results demonstrate the importance of exposed crystalline faces in the photocatalytic activity.

The photocatalytic efficiency of the samples for both, the UVC and visible illumination, can be classified as good since even if there is no type of doping or formation of heterostructures, the photocatalytic activity under visible illumination occurs [23,42–44]. It is possible that the oxygen vacancies, created during the synthesis process, could influence equally as a dopant element in ZnO lattice, to active the visible photocatalytic efficiency [12,14,45,46]. Wang et al. [14] proposed a method to produce ZnO photocatalyst through the conversion of ε-$Zn(OH)_2$ to ZnO in NaOH solutions, rich in oxygen vacancies. However, the synthesis method is time-consuming, required 38 h to obtain ZnO particles. Authors show the superior activities under UV and visible illumination toward the degradation of RhB of the V_O-rich ZnO photocatalyst, attributing the photocatalytic performance through the oxygen vacancies of the material.

Under visible light (Fig. 8B), the samples also exhibited a different behavior. It is expected that, with lower band gap value of the sample, the visible photocatalytic activity increase (Table 4) [47,48]. However, this does not always occur. In this case, the RP sample presented a greater photocatalytic activity in the visible, slightly close to the result submitted for FL sample (Table 4). The RP sample reached 48% of RhB discoloration under visible illumination, and FL sample obtained 52% of RhB discoloration. The percentage of RhB discoloration is influenced by dye sensitizing mechanism under visible illumination, which influences in the photocatalytic efficiency. As the dye sensitizing mechanism is dependent of charge transference from RhB to photocatalyst surface, the morphology might affect the mechanism process. The PL sample shows an interesting behavior under visible illumination (Table 4), with similar behavior as RP and FL samples during the first 60 min of RhB discoloration and, later, photocatalytic efficiency decreases, until obtaining 43% of RhB discoloration. It is possible that a passivation of the PL sample surface occurred, with some sub-product produced during RhB discoloration process, not funding during the UV–vis analysis, adsorbing irreversibly on photocatalytic sites.

In this way, the modification in solvent reaction could alter the morphology and, consequently, the visible photocatalytic activity, as presented by PL and RP samples results and, the precursor solution concentration during the synthesis method did not influence directly in the photocatalytic activity under visible light, as shown by RP and FL samples. Again, BL sample had the lowest efficiency among all the samples, with only 30% of RhB discoloration under visible illumination, confirming the influence of temperature and time reaction in ZnO morphology and visible photocatalytic activity. As for the photocatalytic activity under UVC illumination, the morphology of the ZnO particles must influence the process efficiency, as well as the greater number of exposed faces of the crystals in the samples. The photo-charged carrier recombination is another important factor, even in the visible region, and also the dye sensitizing mechanism. In the case of BL sample, the disorganized morphology and the lowest band gap value could favor the increase in electron-hole pair recombination and disable the surface charge transference between RhB and ZnO particles, reducing the visible photocatalytic activity.

4. Conclusions

The fine control of the MAH synthesis parameters, like temperature, time and solvent of synthesis reaction kept the main ZnO hexagonal wurtzite crystalline phase. However, the zinc precursor concentration, as well as the solvent, time, and temperature of synthesis affect the morphological structure, producing Plates (PL), Rounded Plates (RP), Brush-like (BL) and 3-D flower-like (FL) morphologies. The calculated band gap values for the samples varies from 3.17 to 3.24 eV, with the lowest band gap value for the BL sample, synthesized in a shorter reaction time and higher temperature. The synthesis condition not influenced in the main crystalline phase, presenting as wurtzite for all samples. The photo-charge recombination of Plates and Rounded Plates morphologies show more elevated than for Brush-like and 3-D flower-Like morphologies. The electron transfer rate shows highest value for FL morphology and similar values for another sample. The influence of the addition of ethyl alcohol on ZnO (RP sample) synthesis, without the concentration of precursor solution modification, is similar from the kinetic point of view under UVC illumination and FL samples show an improvement in photocatalytic efficiency. Under visible illumination, the samples presented good photocatalytic results, especially FL and RP samples, even without any doping process during the synthesis, probably caused by the oxygen vacancies promoted during the crystal growth, resulting in a good influence in photocatalytic results.

Acknowledgement

The authors acknowledge the financial support of São Paulo Research Foundation (FAPESP) (grant 2015/04511-5; 2014/17343-0; 2017/01267-1), and of National Council for Scientific and Technological Development (CNPQ) (Proc. 444926/2014-3).

Appendix A. Supplementary data

Supplementary data associated with this article can be found, in the online version, at https://doi.org/10.1016/j.jphotochem.2017.11.032.

References

[1] A.N. Rao, B. Sivasankar, V. Sadasivam, Kinetic studies on the photocatalytic degradation of Direct Yellow 12 in the presence of ZnO catalyst, J. Mol. Catal. A Chem. 306 (2009) 77–81, doi:http://dx.doi.org/10.1016/j.molcata.2009.02.028.

[2] O. Lupan, V.M. Guérin, I.M. Tiginyanu, V.V. Ursaki, L. Chow, H. Heinrich, T. Pauporté, Well-aligned arrays of vertically oriented ZnO nanowires electrodeposited on ITO-coated glass and their integration in dye sensitized solar cells, J. Photochem. Photobiol. A Chem. 211 (2010) 65–73, doi:http://dx.doi.org/10.1016/j.jphotochem.2010.02.004.

[3] G. Biasotto, M.G.A. Ranieri, C.R. Foschini, A.Z. Simões, E. Longo, M.A. Zaghete, Gas sensor applications of zinc oxide thin film grown by the polymeric precursor method, Ceram. Int. 40 (2014) 14991–14996, doi:http://dx.doi.org/10.1016/j.ceramint.2014.06.099.

[4] A. Mhamdi, A. Labidi, B. Souissi, M. Kahlaoui, A. Yumak, K. Boubaker, A. Amlouk, M. Amlouk, Impedance spectroscopy and sensors under ethanol vapors application of sprayed vanadium-doped ZnO compounds, J. Alloys Compd. 639 (2015) 648–658, doi:http://dx.doi.org/10.1016/j.jallcom.2015.03.205.

[5] X. Song, D. Dong, P. Yang, Formation of nanoplate-based clew-like ZnO mesocrystals and their photocatalysis application, RSC Adv. 6 (2016) 51544–51551, doi:http://dx.doi.org/10.1039/C6RA07874E.

[6] X.G. Han, H.Z. He, Q. Kuang, X. Zhou, X.H. Zhang, T. Xu, Z.X. Xie, L.S. Zheng, Controlling morphologies and tuning the related properties of nano/microstructured ZnO crystallites, J. Phys. Chem. C. 113 (2009) 584–589, doi:http://dx.doi.org/10.1021/jp808233e.

[7] I.M.P. Silva, G. Byzynski, C. Ribeiro, E. Longo, Different dye degradation mechanisms for ZnO and ZnO doped with N (ZnO:N), J. Mol. Catal. A Chem. 417 (2016) 89–100, doi:http://dx.doi.org/10.1016/j.molcata.2016.02.027.

[8] A.P. de Moura, R.C. Lima, M.L. Moreira, D.P. Volanti, J.W.M. Espinosa, M.O. Orlandi, P.S. Pizani, J.A. Varela, E. Longo, ZnO architectures synthesized by a microwave-assisted hydrothermal method and their photoluminescence properties, Solid State Ionics 181 (2010) 775–780, doi:http://dx.doi.org/10.1016/j.ssi.2010.03.013.

[9] P.-S. Shen, C.-M. Tseng, T.-C. Kuo, C.-K. Shih, M.-H. Li, P. Chen, Microwave-assisted synthesis of titanium dioxide nanocrystalline for efficient dye-sensitized and perovskite solar cells, Sol. Energy 120 (2015) 345–356, doi:http://dx.doi.org/10.1016/j.solener.2015.07.036.

[10] S.H. Cho, H.H. Nguyen, G. Gyawali, J.-E. Son, T. Sekino, B. Joshi, S.H. Kim, Y.H. Jo, T.H. Kim, S.W. Lee, Effect of microwave-assisted hydrothermal process parameters on formation of different TiO2 nanostructures, Catal. Today 266 (2016) 46–52, doi:http://dx.doi.org/10.1016/j.cattod.2015.10.001.

[11] L. Schmidt-mende, J.L. Macmanus-driscoll, ZnO – nanostructures, defects, and devices, Mater. Today 10 (2007) 40–48, doi:http://dx.doi.org/10.1016/S1369-7021(07)70078-0.

[12] M. Samadi, M. Zirak, A. Naseri, E. Khorashadizade, A.Z. Moshfegh, Recent progress on doped ZnO nanostructures for visible-light photocatalysis, Thin Solid Films. (2016), doi:http://dx.doi.org/10.1016/j.tsf.2015.12.064.

[13] S.G. Kumar, K.S.R.K. Rao, Zinc oxide based photocatalysis: tailoring surface-bulk structure and related interfacial charge carrier dynamics for better environmental applications, RSC Adv. 5 (2015) 3306–3351, doi:http://dx.doi.org/10.1039/C4RA13299H.

[14] J. Wang, R. Chen, Y. Xia, G. Wang, H. Zhao, L. Xiang, S. Komarneni, Cost-effective large-scale synthesis of oxygen-defective ZnO photocatalyst with superior activities under UV and visible light, Ceram. Int. 43 (2017) 1870–1879, doi:http://dx.doi.org/10.1016/j.ceramint.2016.10.146.

[15] M.A. Behnajady, N. Modirshahla, R. Hamzavi, Kinetic study on photocatalytic degradation of C.I. acid yellow 23 by ZnO photocatalyst, J. Hazard. Mater. 133 (2006) 226–232, doi:http://dx.doi.org/10.1016/j.jhazmat.2005.10.022.

[16] G. Byzynski, C. Melo, D.P. Volanti, M.M. Ferrer, A.F. Gouveia, C. Ribeiro, J. Andrés, E. Longo, The interplay between morphology and photocatalytic activity in ZnO and N-doped ZnO crystals, Mater. Des. (2017), doi:http://dx.doi.org/10.1016/j.matdes.2017.02.020.

[17] F.A. Kröger, H.J. Vink, Relations between the concentrations of imperfections in crystalline solids, Solid State Phys. Adv. Res. Appl. 3 (1956) 307–435, doi:http://dx.doi.org/10.1016/S0081-1947(08)60135-6.

[18] F.A. Kröger, H.J. Vink, Relations between the concentrations of imperfections in solids, J. Phys. Chem. Solids. 5 (1958) 208–223, doi:http://dx.doi.org/10.1016/0022-3697(58)90069-6.

[19] Yuanhui Zheng, Chongqi Chen, Yingying Zhan, Xingyi Lin, Qi Zheng, Kemei Wei, Jiefang Zhu, Y. Zhu, Luminescence and photocatalytic activity of ZnO nanocrystals, Correl. Between Struct. Property (2007), doi:http://dx.doi.org/10.1021/IC062394M.

[20] Y. Zheng, C. Chen, Y. Zhan, X. Lin, Q. Zheng, K. Wei, J. Zhu, Photocatalytic activity of Ag/ZnO heterostructure nanocatalyst: correlation between structure and property, J. Phys. Chem. C. 112 (2008) 10773–10777, doi:http://dx.doi.org/10.1021/jp8027275.

[21] C.B. Ong, L.Y. Ng, A.W. Mohammad, A review of ZnO nanoparticles as solar photocatalysts: synthesis, mechanisms and applications, Renew. Sustain. Energy Rev. 81 (2018) 536–551, doi:http://dx.doi.org/10.1016/j.rser.2017.08.020.

[22] J.A. Aguilar-Martínez, M.I. Pech Canul, M.B. Hernández, A.B. Glot, E. Rodríguez, L. García Ortiz, Effect of sintering temperature on the electric properties and microstructure of SnO2-Co3O4-Sb2O5-Cr2O3 varistor ceramic, Ceram. Int. 39 (2013) 4407–4412, doi:http://dx.doi.org/10.1016/j.ceramint.2012.11.030.

[23] U. Alam, A. Khan, W. Raza, A. Khan, D. Bahnemann, M. Muneer, Highly efficient Y and V co-doped ZnO photocatalyst with enhanced dye sensitized visible light photocatalytic activity, Catal. Today 284 (2017) 169–178, doi:http://dx.doi.org/10.1016/j.cattod.2016.11.037.

[24] Z. Yan, X. Yu, Y. Zhang, H. Jia, Z. Sun, P. Du, Enhanced visible light-driven hydrogen production from water by a noble-metal-free system containing organic dye-sensitized titanium dioxide loaded with nickel hydroxide as the cocatalyst, Appl. Catal. B Environ. 160 (2014) 173–178, doi:http://dx.doi.org/10.1016/j.apcatb.2014.05.017.

[25] Elson Longo da Silva, José Arana Varela, David Keyson de Araújo Almeida, Diogo Paschoalini Volanti, E. Longo Da Silva, J. Arana Varela, D.K. De Araujo Almeida, D. Paschoalini Volanti, Aided Device for Hydrothermal Synthesis of Nanostructured Oxides, Particularly Obtaining Particles of Metal Oxides, Comprises Container, in Which Hydrothermal Reaction Takes Place, and Lid for Container, BR200815393-A2, (2010) .

[26] T. Engel, P. Reid, Physical Chemistry, (2014) .

[27] P. Atkin, J. Paula, Physical Chemistry, (2006), doi:http://dx.doi.org/10.1039/C1CS15191F.

[28] H. Xu, Z. Wu, M. Ding, X. Gao, Microwave-assisted synthesis of flower-like BN/BiOCl composites for photocatalytic Cr(VI) reduction upon visible-light irradiation, Mater. Des. (2016), doi:http://dx.doi.org/10.1016/j.matdes.2016.10.057.

[29] M. Navaneethan, J. Archana, Y. Hayakawa, Morphological evolution of monodispersed ZnO nanorods to 3 dimensional hierarchical flowers by hydrothermal growth, CrystEngComm 15 (2013) 8246, doi:http://dx.doi.org/10.1039/c3ce41601a.

[30] S. Bakardjieva, V. Stengl, L. Szatmary, J. Subrt, J. Lukac, N. Murafa, D. Niznansky, K. Cizek, J. Jirkovsky, N. Petrova, Transformation of brookite-type TiO2 nanocrystals to rutile: correlation between microstructure and photoactivity, J. Mater. Chem. 16 (2006) 1709, doi:http://dx.doi.org/10.1039/b514632a.

[31] J. Chen, D. Li, J. Wang, P. Wang, C. Cao, Y. Shao, J. Wang, J. Xian, Morphological effect on photocatalytic degradation of Rhodamine B and conversion of active species over BaSb2O6, Appl. Catal. B Environ. 163 (2015) 323–329, doi:http://dx.doi.org/10.1016/j.apcatb.2014.08.014.

[32] Z.L. Wang, Zinc oxide nanostructures: growth, properties and applications, J. Phys. Condenced Matter. 16 (2004) R829–R858, doi:http://dx.doi.org/10.1088/0953-8984/16/25/R01.

[33] A.B. Murphy, Band-gap determination from diffuse reflectance measurements of semiconductor films, and application to photoelectrochemical water-splitting, Sol. Energy Mater. Sol. Cells. 91 (2007) 1326–1337, doi:http://dx.doi.org/10.1016/j.solmat.2007.05.005.

[34] X.-Y. Li, H.-J. Li, Z.-J. Wang, H. Xia, Z.-Y. Xiong, J.-X. Wang, B.-C. Yang, Effect of substrate temperature on the structural and optical properties of ZnO and Al-doped ZnO thin films prepared by dc magnetron sputtering, Opt. Commun. 282 (2009) 247–252, doi:http://dx.doi.org/10.1016/j.optcom.2008.10.003.

[35] E.S. Tuzemen, K. Kara, S. Elagoz, D.K. Takci, I. Altuntas, R. Esen, Structural and electrical properties of nitrogen-doped ZnO thin films, Appl. Surf. Sci. 2014 (2016) 157–163, doi:http://dx.doi.org/10.1016/j.apsusc.2014.02.118.

[36] K. Ocakoglu, S.A. Mansour, S. Yildirimcan, A.A. Al-Ghamdi, F. El-Tantawy, F. Yakuphanoglu, Microwave-assisted hydrothermal synthesis and characterization of ZnO nanorods, Spectrochim. Acta Part A Mol. Biomol. Spectrosc. 148 (2015) 362–368, doi:http://dx.doi.org/10.1016/j.saa.2015.03.106.

[37] K.N. Abbas, N. Bidin, R.S. Sabry, Controllable ZnO nanostructures evolution via synergistic pulsed laser ablation and hydrothermal methods, Ceram. Int. 42 (2016) 13535–13546, doi:http://dx.doi.org/10.1016/j.ceramint.2016.05.146.

[38] D. Martín-Yerga, E.C. Rama, A. Costa-García, Electrochemical characterization of ordered mesoporous carbon screen-printed electrodes, J. Electrochem. Soc. 163 (2016) B176–B179, doi:http://dx.doi.org/10.1149/2.0871605jes.

[39] G.B. Soares, R.A.P. Ribeiro, S.R. de Lazaro, C. Ribeiro, Photoelectrochemical and theoretical investigation of the photocatalytic activity of TiO $_2$: N, RSC Adv. 6 (2016) 89687–89698, doi:http://dx.doi.org/10.1039/C6RA15825 K.

[40] I.A. Castro, G. Byzynski, M. Dawson, C. Ribeiro, Charge transfer mechanism of WO3/TiO2 heterostructre for photoelectrochemical water splitting, J. Photochem. Photobiol. A Chem. (2017), doi:http://dx.doi.org/10.1016/j.jphotochem.2017.02.024.

[41] V.R. Shinde, T.P. Gujar, T. Noda, D. Fujita, A. Vinu, M. Grandcolas, J. Ye, Growth of shape- and size-selective zinc oxide nanorods by a microwave-assisted chemical bath deposition method: effect on photocatalysis properties, Chem. A Eur. J. 16 (2010) 10569–10575, doi:http://dx.doi.org/10.1002/chem.200903370.

[42] S.-Y. Pung, W.-P. Lee, A. Aziz, Kinetic study of organic dye degradation using ZnO particles with different morphologies as a photocatalyst, Int. J. Inorg. Chem. 2012 (2012) 1–9, doi:http://dx.doi.org/10.1155/2012/608183.

[43] Q. Luo, X. Yang, X. Zhao, D. Wang, R. Yin, X. Li, J. An, Facile preparation of well-dispersed ZnO/cyclized polyacrylonitrile nanocomposites with highly enhanced visible-light photocatalytic activity, Appl. Catal. B Environ. 204 (2017) 304–315, doi:http://dx.doi.org/10.1016/j.apcatb.2016.11.037.

[44] S. Le, T. Jiang, Y. Li, Q. Zhao, Y. Li, W. Fang, M. Gong, Highly efficient visible-light-driven mesoporous graphitic carbon nitride/ZnO nanocomposite photocatalysts, Appl. Catal. B Environ. 200 (2017) 601–610, doi:http://dx.doi.org/10.1016/j.apcatb.2016.07.027.
[45] L. Xu, Y.L. Hu, C. Pelligra, C.H. Chen, L. Jin, H. Huang, S. Sithambaram, M. Aindow, R. Joesten, S.L. Suib, ZnO with different morphologies synthesized by solvothermal methods for enhanced photocatalytic activity, Chem. Mater. 21 (2009) 2875–2885, doi:http://dx.doi.org/10.1021/cm900608d.
[46] A.V. Emeline, V.N. Kuznetsov, V.K. Ryabchuk, N. Serpone, On the way to the creation of next generation photoactive materials, Environ. Sci. Pollut. Res. 19 (2012) 3666–3675, doi:http://dx.doi.org/10.1007/s11356-011-0665-3.
[47] T. Yoshida, S. Niimi, M. Yamamoto, T. Nomoto, S. Yagi, Effective nitrogen doping into TiO2 (N-TiO2) for visible light response photocatalysis, J. Colloid Interface Sci. 447 (2015) 278–281, doi:http://dx.doi.org/10.1016/j.jcis.2014.12.097.
[48] J. Arul Mary, J. Judith Vijaya, M. Bououdina, L. John Kennedy, J.H. Daie, Y. Song, Investigation of structural, surface morphological, optical properties and first-principles study on electronic and magnetic properties of (Ce, Fe)-co doped ZnO, Phys. B Condens. Matter. 456 (2015) 344–354, doi:http://dx.doi.org/10.1016/j.physb.2014.09.023.